Solving Einstein's equations as Bayesian inference

Frederik De Ceuster — *Leuven Gravity Institute, Department of Physics & Astronomy, KU Leuven, Belgium*
Tom Colemont — *Leuven Gravity Institute, Department of Electrical Engineering, KU Leuven, Belgium*
Tjonnie G.F. Li — *Leuven Gravity Institute, Department of Physics & Astronomy, KU Leuven, Belgium*

Abstract

Gravitational waves (GWs) are revolutionising our fundamental understanding of physics and cosmology. However, the numerical modelling required to turn their measurements into scientific detections poses a formidable computational challenge. In this paper, we explore the feasibility of probabilistic numerics (PN) to model GW sources. As a proof-of-principle, we pose the solution of the Einstein equations, which relate the dynamics of spacetime to its matter content, as a Bayesian inference problem. Using a fixed-point iteration scheme and iterative linearisation, we show that the non-linear problem can be divided into a set of consecutively solvable Bayesian linear regression problems. As a first application, we use this approach to solve the spacetime geometry inside a static and spherically-symmetric neutron star. We conclude that PN provides a promising approach to overcome some of the computational challenges in GW science.

Proceedings of the 1st International Conference on Probabilistic Numerics (ProbNum) 2025,
Sophia Antipolis, France. PMLR Volume 271.

1 Introduction

The general theory of relativity (GR; Einstein, 1916) is currently our best theory of gravity. For more than a century, it has been consistent with all experiments and observations (Will, 2014; Ishak, 2018; Abbott et al., 2016b, 2019). In GR, gravity is described as a result of curvature in the fabric of spacetime. Among its most profound predictions are gravitational waves (GWs): curvature oscillations in spacetime. Their first direct detection (Abbott et al., 2016a), opened up a whole new window on the universe, enabling us to probe elusive astrophysical objects like black holes and cosmic events like the Big Bang more closely than with any other kind of observation. The next generation of GW observatories, such as the Einstein Telescope (in Europe), Cosmic Explorer (in the US), and LISA (in space), will have significantly increased sensitivities compared to current detectors, poising them to revolutionize our fundamental understanding of physics and cosmology. However, the modelling required to turn their measurements into scientific detections poses a formidable computational challenge.

The challenge in GW modelling is twofold. On the one hand, the increased sensitivity of GW observatories puts higher accuracy requirements on waveform models. Failing to meet these requirements leads to mismatches between modelled and observed signals, which biases the parameter estimation (Pürrer and Haster, 2020). On the other hand, currently, well-understood waveform models only exist for coalescing binary systems that can be modelled efficiently in a semi-analytical way (see e.g. Blanchet, 2024). This ignores a significant part of all possibly observed GW signals, such as GW bursts from supernovae, that could be discovered with future detectors (see e.g. Maggiore et al., 2020). This new kind of waveforms can only be modelled with computationally expensive numerical simulations that cannot be generated efficiently enough to explore the relevant parameter space. Hence, new GW discoveries are critically constrained by our ability to model GW sources.

GW source models simulate the dynamics of matter in a dynamical spacetime. Spacetime is described by general relativity (GR), while matter can be described with general-relativistic hydrodynamics (GRHD). As J.A. Wheeler famously put it: "Matter tells spacetime how to curve, while spacetime tells matter how to move." In this paper, we will focus on the first part and devise a solver for the spacetime geometry, given its matter content. Specifically, we will pose the solution of the Einstein equations as a Bayesian inference problem. Using probabilistic numerics (PN; Hennig et al., 2015, 2022; Cockayne et al., 2019), we later hope to leverage the control over uncertainties to find new optimisation opportunities, to help us push the trade-off between computational speed and accuracy. In addition, the Bayesian view of PN might help to better connect GW source modelling to the advanced data analysis that is required to measure GW signals. Conversely, due to the mathematical richness of GR, it might provide unique opportunities to develop new PN methods, leveraging the mathematical structure and symmetries in GR.

To make this paper more accessible, we have tried to avoid heavy notation, typical for GR. Hence, throughout this paper, $\boldsymbol{\nabla}$, denotes the ordinary gradient, known from vector calculus, and, $\nabla^2 \equiv \boldsymbol{\nabla} \cdot \boldsymbol{\nabla}$, denotes the Laplacian. Vectors are denoted by boldface but not necessarily lower-case symbols ($\boldsymbol{a}$), matrices are denoted by sans-serif capitals (A), and we use a dot ($\cdot$) to explicitly denote Euclidean inner-products between vectors.

The structure of this paper is as follows. In Section 2, we describe the specific problem we aim to address. In Section 3, we introduce our probabilistic solution and some simplifying assumptions. Section 4 provides an application of the probabilistic numerical method to a static, spherically-symmetric neutron star, and, finally, in Sections 5 and 6 we discuss our results and conclude.

2 Problem Statement

The Einstein equations relate the geometry of spacetime to the energy and momentum of its matter content. For simplicity, we will not solve the exact equations but rather resort to a waveless approximation (Isenberg, 2008; Wilson and Mathews, 1989). This is valid, as long as only a limited amount of energy and momentum is carried by GWs. It is used e.g. to model neutron stars, where most of the energy and momentum is carried by the matter anyway. In this approximation, the spacetime geometry, $\boldsymbol{\mathcal{G}} \equiv (\alpha, \boldsymbol{\beta}, \psi)$, is defined by two scalar functions, α and ψ, and one 3-vector function, $\boldsymbol{\beta}$. All are functions of both time and space, $(t, \boldsymbol{x})$. Together they define the spacetime metric, a rank-2 tensor, which can be represented by a line element,

$$\mathrm{d}s^2 \;=\; -\alpha^2 \mathrm{d}t^2 \,+\, \psi^4 \left(\mathrm{d}\boldsymbol{x} + \boldsymbol{\beta}\,\mathrm{d}t\right)^2 . \tag{1}$$

This can be thought of as the infinitesimal spacetime displacement, $\mathrm{d}s$, corresponding to the infinitesimal coordinate displacements, $\mathrm{d}t$, in time, and $\mathrm{d}\boldsymbol{x}$, in space. We will work in the xCFC formulation from Cordero-Carrión et al. (2009). In this formulation, the Einstein equations, in which matter ($\boldsymbol{\mathcal{M}}$) tells spacetime ($\boldsymbol{\mathcal{G}}$) how to curve, can be written as a set of four coupled, non-linear, elliptic partial differential equations,

$$\nabla^2 \boldsymbol{X} \,+\, \frac{1}{3}\boldsymbol{\nabla}\left(\boldsymbol{\nabla}\cdot\boldsymbol{X}\right) \;=\; \boldsymbol{S}_{\boldsymbol{X}} \tag{2}$$

$$\nabla^2 \psi \;=\; S_\psi \left[\boldsymbol{X}, \psi\right] \tag{3}$$

$$\nabla^2 \left(\alpha\psi\right) \;=\; S_{\alpha\psi}\left[\boldsymbol{X}, \psi, \alpha\right] \tag{4}$$

$$\nabla^2 \boldsymbol{\beta} \,+\, \frac{1}{3}\boldsymbol{\nabla}\left(\boldsymbol{\nabla}\cdot\boldsymbol{\beta}\right) \;=\; \boldsymbol{S}_{\boldsymbol{\beta}}\left[\boldsymbol{X}, \psi, \alpha\right] \tag{5}$$

Here, $\boldsymbol{X}$, is a 3-vector function that helps decouple the equations while ensuring a unique solution. The source functions on the right-hand sides encode the matter distribution, $\boldsymbol{\mathcal{M}} \equiv (E, \boldsymbol{P}, P)$, which is defined by two scalar functions, E and P, and one 3-vector function, $\boldsymbol{P}$. These are projections of the energy-momentum tensor of the matter, and we assume that we can access them through another solver. To emphasize the non-linearity and coupling between the equations, we explicitly indicated the dependence of each source function on the other metric functions. The source functions read,

$$\boldsymbol{S}_{\boldsymbol{X}} \;\equiv\; 8\pi\,\boldsymbol{P} \tag{6}$$

$$S_\psi\left[\boldsymbol{X}, \psi\right] \;\equiv\; -2\pi\,E/\psi \,-\, \frac{1}{8}\,\mathsf{A}^2/\psi^7 \tag{7}$$

$$S_{\alpha\psi}\left[\boldsymbol{X}, \psi, \alpha\right] \;\equiv\; 2\pi\,\alpha\left(E + 2P\right)/\psi \,+\, \frac{7}{8}\,\alpha\,\mathsf{A}^2/\psi^7 \tag{8}$$

$$\boldsymbol{S}_{\boldsymbol{\beta}}\left[\boldsymbol{X}, \psi, \alpha\right] \;\equiv\; 16\pi\,\boldsymbol{P}\,\alpha/\psi^6 \,+\, 2\,\mathsf{A}\boldsymbol{\nabla}\left(\alpha/\psi^6\right) \tag{9}$$

where we defined the auxiliary matrix functions,

$$\mathsf{A} \;\equiv\; \boldsymbol{\nabla}\boldsymbol{X} \,+\, \left(\boldsymbol{\nabla}\boldsymbol{X}\right)^{\mathrm{T}} \,-\, \frac{2}{3}\left(\boldsymbol{\nabla}\cdot\boldsymbol{X}\right)1, \tag{10}$$

$$\mathsf{A}^2 \;\equiv\; \mathrm{Tr}\left(\mathsf{A}\,\mathsf{A}^{\mathrm{T}}\right). \tag{11}$$

As boundary conditions, we typically assume that most of the matter is at the centre of the model, far away from the boundary, such that the metric on the boundary can be approximated by a Schwarzschild geometry, which in isotropic coordinates reads,

$$\psi \;=\; 1 \,+\, M/(2r), \tag{12}$$

$$\alpha\psi \;=\; 1 \,-\, M/(2r), \tag{13}$$

while the vector fields vanish, $\boldsymbol{X} = \boldsymbol{\beta} = \boldsymbol{0}$. Here, the constant, M, denotes the total mass in the model. If this is unknown, the conditions can be recast in terms of derivatives of the fields.

The decoupling between Eqs. (2–5) is such that they can be solved one after the other. This means that given the matter distribution ($\boldsymbol{\mathcal{M}}$) throughout space at some time, t, we can solve Eqs. (2–5) step-by-step to obtain the geometry ($\boldsymbol{\mathcal{G}}$) throughout space at that time. Once the geometry is determined, we can evolve the matter over a time step, δt, to obtain the new matter distribution at a later time, $t + \delta t$, and so on.

Typically, Eqs. (2–5) are solved using standard non-linear multigrid solvers (see e.g. Cheong et al., 2020, 2021). In principle, the metric should be updated after every update of the matter dynamics, since this changes the source functions. However, in practice, it turns out that the metric only changes very little over a single time step, δt. This is related to the fact that the metric is always smoother than the source functions. This can be understood, since the differential operators appearing in Eqs. (2–5) are the scalar Laplacian and a slight variation on the vector Laplacian, for which the solutions are convolutions of the source functions with a smoothing kernel. To limit the computational cost, the metric is typically only computed after a number of time-steps in the matter dynamics. When exactly to compute the metric is sometimes determined by an empirically-defined fixed number of time-steps in the matter dynamics (~ 50), or is determined dynamically, for instance, by a criterion on the residual of Eq. (3), as done e.g. in Cheong et al. (2021).

Finally, we note that evaluating the source functions ($\boldsymbol{\mathcal{M}}$) often poses a significant computational bottleneck (see e.g. Newman and Hamlin, 2014). The bottleneck stems from the inversions of non-linear equations that relate the "primitive variables" that appear in the source functions ($\boldsymbol{\mathcal{M}}$) to the "conserved variables" that are evolved in the matter dynamics. To limit the required number of evaluations of the source functions, since we know the metric is smoother than the sources, Eqs. (2–5) are often solved using a coarser spatial discretisation than the matter dynamics.

In this paper, we explore whether the xCFC formulation of the Einstein equations (2–5) can be solved in a probabilistic numerical way. Our ultimate goal is to leverage the resulting control over uncertainties to optimize the solver, e.g. by dynamically deciding whether, where, and at what resolution the geometry should be updated. As a first step, in this paper, we solve the equations as a Bayesian inference problem. Later, we will use this to optimise the solver. As such, this is a first step towards probabilistic numerical relativity (PNR) and mainly serves as a proof-of-principle that PN can also be applied to solve the mathematically challenging but rich Einstein equations.

3 Bayesian Solution Method

To introduce the probabilistic numerical approach, we abstract equations (2–5), and write them as,

$$\mathscr{L} f(\boldsymbol{x}) \;=\; S[f](\boldsymbol{x}) \tag{14}$$

in which, $\mathscr{L}$, is a linear differential operator, and the square brackets on S denote its functional dependence on f, which can be non-linear. For clarity of notation, we present the approach for scalar functions, however, vector functions can be treated in a very similar way.

3.1 Discretisation

We start with a spectral discretisation of the solution, i.e. we express each metric function ($\boldsymbol{X}$, ψ, $\alpha\psi$, and $\boldsymbol{\beta}$) as a linear combination of basis functions, ϕ_n,

$$f(\boldsymbol{x}) \;=\; \sum_{n=1}^{N} w_n \, \phi_n(\boldsymbol{x}). \tag{15}$$

Next, we discretise the functions in the spatial domain by introducing a set of collocation points $\{\boldsymbol{x}_d\}_{d=1}^{D}$. This allows us to define the basis function matrix, $\mathsf{F} \in \mathbb{R}^{D\times N}$, with entries, $\mathsf{F}_{dn} \equiv \phi_n(\boldsymbol{x}_d)$. The spectral expansion (Eq. 15) evaluated at these collocation points, then reads,

$$\mathsf{F}\,\boldsymbol{w} = \boldsymbol{f} \tag{16}$$

in which $(\boldsymbol{w})_n \equiv w_n$ are the weights and $(\boldsymbol{f})_d \equiv f(\boldsymbol{x}_d)$ are the function evaluations at the collocation points.

In principle, we can choose a different basis for each metric variable. However, we will use one basis set for the scalar and another set for the vector variables. The choice of basis functions can largely be guided by the differential operators that act on them. For instance, the eigenfunctions of these operators offer a convenient choice. We will construct these in Section 3.6.

Classically, solving the Einstein equations comes down to computing a (deterministic) solution for the weights, w_n, for each metric function. In contrast, PN aims to determine a probability distribution over these weights, such that the mean corresponds to the classical result and the width of the distribution can be interpreted as the uncertainty on that result.

3.2 Fixed-point Iteration

The left-hand sides of the xCFC equations (2–5) contain two different linear differential operators, one scalar and one vector. The source functions on the right-hand sides are linear in the matter functions ($\boldsymbol{\mathcal{M}}$), but non-linear in the metric functions ($\boldsymbol{\mathcal{G}}$). We will handle this non-linearity in an iterative way, dividing the problem in a set of linear sub-problems.

Equation (2) is linear and can readily be solved as a linear Bayesian regression problem, which we will detail in Section 3.3. However, the source functions in equations (3–5) all depend in a non-linear way on the metric functions. Given an initial guess, we can handle the non-linearity through fixed-point iteration, following the notation of equation (14), this yields,

$$\mathscr{L} f_{(k)} \;=\; S\big[f_{(k-1)}\big]. \tag{17}$$

In this way, each iteration requires solving only a linear problem, by linearity of $\mathscr{L}$. In our setting, a natural choice for the initial guess in the iterative process for each of the metric functions can be obtained from the previous hydrodynamic time step, since we expect only small variations between successive steps. It remains to solve these linear (sub-)problems in a probabilistic way.

3.3 Bayesian linear regression

Each linear (discretised) sub-problem can be written as,

$$\mathsf{L}\,\boldsymbol{w} \;=\; \boldsymbol{S}, \tag{18}$$

in which $\mathsf{L}_{dn} \equiv (\mathscr{L}\phi_n)(\boldsymbol{x}_d)$ is the design matrix and $\boldsymbol{S}_d \equiv S(\boldsymbol{x}_d)$ is the source function evaluation. This can be solved as a Bayesian linear regression problem (see e.g. De Ceuster et al., 2023). For simplicity, we assume a Gaussian prior over the spectral weights,

$$p(\boldsymbol{w}) \;=\; \mathcal{N}\big(\boldsymbol{\mu}_{\boldsymbol{w}}, \Sigma_{\boldsymbol{w}}\big), \tag{19}$$

with mean, $\boldsymbol{\mu}_{\boldsymbol{w}}$, and covariance, $\Sigma_{\boldsymbol{w}}$, and a Gaussian likelihood for the observations of the source term,

$$p(\boldsymbol{S}\,|\,\boldsymbol{w}) \;=\; \mathcal{N}\big(\mathsf{L}\,\boldsymbol{w}, \Sigma_{\boldsymbol{S}}\big). \tag{20}$$

The covariance matrix, $\Sigma_{\boldsymbol{S}}$, can be used to represent the uncertainty associated with the source function, $\boldsymbol{S}$, which can, for instance, account for the uncertainty from the solver through which they were obtained. In Section 3.4, we detail how this covariance matrix, $\Sigma_{\boldsymbol{S}}$, can be obtained or approximated for non-linear source functions. The resulting posterior distribution over the weights, given the source, is also Gaussian and reads,

$$p(\boldsymbol{w}\,|\,\boldsymbol{S}) \;=\; \mathcal{N}\left(\boldsymbol{\mu}_{\boldsymbol{w}|\boldsymbol{S}}, \Sigma_{\boldsymbol{w}|\boldsymbol{S}}\right), \tag{21}$$

with the posterior mean and covariance given by,

$$\boldsymbol{\mu}_{\boldsymbol{w}|\boldsymbol{S}} \;=\; \Sigma_{\boldsymbol{w}|\boldsymbol{S}}\left(\,\mathsf{L}^{\mathrm{T}}\,\Sigma_{\boldsymbol{S}}^{-1}\,\boldsymbol{S} \;+\; \Sigma_{\boldsymbol{w}}^{-1}\boldsymbol{\mu}_{\boldsymbol{w}}\right), \tag{22}$$

$$\Sigma_{\boldsymbol{w}|\boldsymbol{S}} \;=\; \left(\Sigma_{\boldsymbol{w}}^{-1} \;+\; \mathsf{L}^{\mathrm{T}}\,\Sigma_{\boldsymbol{S}}^{-1}\,\mathsf{L}\right)^{-1} \tag{23}$$

As a result, the solution of the linear sub-problem at the collocation points is therefore also Gaussian,

$$p(\boldsymbol{f}\,|\,\boldsymbol{S}) \;=\; \mathcal{N}\left(\boldsymbol{\mu}_{\boldsymbol{f}|\boldsymbol{S}}, \Sigma_{\boldsymbol{f}|\boldsymbol{S}}\right) \tag{24}$$

in which the mean and covariance are given by,

$$\boldsymbol{\mu}_{\boldsymbol{f}|\boldsymbol{S}} \;=\; \mathsf{F}\;\boldsymbol{\mu}_{\boldsymbol{w}|\boldsymbol{S}}, \tag{25}$$

$$\Sigma_{\boldsymbol{f}|\boldsymbol{S}} \;=\; \mathsf{F}\;\Sigma_{\boldsymbol{w}|\boldsymbol{S}}\;\mathsf{F}^{\mathrm{T}}. \tag{26}$$

Throughout the iterations described in equation (17), we fix the prior (Eq. 19), i.e. we use the same $\boldsymbol{\mu}_{\boldsymbol{w}}$ and $\Sigma_{\boldsymbol{w}}$, for each iteration, and only update the covariance, $\Sigma_{\boldsymbol{S}}$, of the likelihood (Eq. 20). Since the source function can be non-linear, we linearize it to approximate the covariance of the likelihood.

3.4 Linearisation of Sources

To propagate the distributions over the matter sources and the metric functions through the non-linear source functions on the right-hand sides of the xCFC equations (Eqs. 2–5), we make a linear approximation of them around the current best estimate,

$$S[\mathcal{G}] \;\approx\; S[\mathcal{G}_0] \;+\; \sum_{g\,\in\,\mathcal{G}} \partial_g S[\mathcal{G}_0]\,(g - g_0), \tag{27}$$

in which, $\mathcal{G}$, denotes the set of variables of the source function, and, $\mathcal{G}_0$ denotes the instances of this set of variables around which we expand. Using this, we can construct the covariance matrix for the source function from the covariance matrices of its variables,

$$\Sigma_{\boldsymbol{S}} \;=\; \sum_{g\,\in\,\mathcal{G}} \mathsf{J}_g\,\Sigma_g\,\mathsf{J}_g{}^{\mathrm{T}} \tag{28}$$

where the Jacobians for each variable, g, are defined as,

$$(\mathsf{J}_g)_{db} \;\equiv\; \partial_g S[\mathcal{G}_0]\,(r_d)\;\delta_{db}. \tag{29}$$

Now we have all building blocks to solve the xCFC equations in a probabilistic numerical way. However, in the following two sections, we add the assumption of spherical symmetry and choose a specific set of basis functions to be able to present a concrete application.

3.5 Spherical Symmetry

The assumption of spherical symmetry is not strictly necessary for what follows, but it greatly simplifies the implementation of our methods and is already sufficient for certain applications (see e.g. Section 4). Moreover, it is appealing, since the waveless approximation that we made, resulting in the xCFC formulation (Eqs. 2–5), is exact rather than an approximation for spherically-symmetric geometries.

In spherical symmetry, the vector source function will always be strictly radial, i.e. in spherical coordinates $\boldsymbol{P} = (P_r, 0, 0)$. As a result, also the vector functions in the metric, $\boldsymbol{X}$ and $\boldsymbol{\beta}$, are strictly radial. From here on, we only consider the radial components of spatial vectors without explicitly denoting it. As boundary condition at the origin ($r = 0$), we require that the radial component of the vector fields vanishes, such that there is no flow through the origin, while, for the scalar fields, it suffices to be regular, i.e. to have a vanishing radial derivative. As stated before, at the outer boundary, we assume that the geometry tends to Schwarzschild, i.e. scalars tend to Eqs. (12–13), while vectors vanish.

In spherical coordinates, assuming spherical symmetry, the relevant components of the differential operators on the left-hand sides of the xCFC equations (2–5) read,

$$\mathscr{L}^{\mathrm{vec}} \;\equiv\; \frac{4}{3}\left(\partial_r^2 \;+\; \frac{2}{r}\,\partial_r \;-\; \frac{2}{r^2}\right) \tag{30}$$

$$\mathscr{L}^{\mathrm{sca}} \;\equiv\; \partial_r^2 \;+\; \frac{2}{r}\,\partial_r. \tag{31}$$

Now, we can define a convenient set of basis functions, using the eigenfunctions of these operators.

3.6 Basis functions

The spectral discretisation requires the choice of a set of basis function (see Section 3.1). The solution of the differential equations can greatly be simplified if we use the eigenfunctions of the relevant differential operators as basis functions.

The eigenfunctions for the vector operator (30), that satisfy the boundary conditions $\phi_n^{\mathrm{vec}}(0) = \phi_n^{\mathrm{vec}}(R) = 0$, are given by,

$$\phi_n^{\mathrm{vec}}(r) \;=\; r\; j_1\big(\sqrt{\lambda_n}\,r/R\big). \tag{32}$$

Here, we used the first-order spherical Bessel function of the first kind, defined as,

$$j_1(r) \;\equiv\; \frac{\sin(r)}{r^2} \;-\; \frac{\cos(r)}{r}, \tag{33}$$

and $\sqrt{\lambda_n}$, are the roots[1] of the Bessel function, j_1, which can readily be computed numerically. The corresponding eigenvalues for the operator (30), are, $4\lambda_n/3$, such that the design matrices read,

$$\mathsf{L}_{dn}^{\mathrm{vec}} \;=\; \frac{4}{3}\,\lambda_n\;\mathsf{F}_{dn}^{\mathrm{vec}}, \tag{34}$$

where $\mathsf{F}_{dn}^{\mathrm{vec}} \equiv \phi_n^{\mathrm{vec}}(r_d)$. Note that, due to this choice of basis functions, the columns of the design matrix are scaled versions of those of the basis function matrix.

For the scalar equations, since we already know their value at the outer boundary (Eqs. 12–13, at $r = R$), it is more convenient to solve them for,

$$\tilde{\psi} \;\equiv\; \psi \;-\; \psi(R) \tag{35}$$

$$\widetilde{\alpha\psi} \;\equiv\; \alpha\psi \;-\; (\alpha\psi)(R) \tag{36}$$

such that these sought-after functions, vanish at the outer boundary. The eigenfunctions corresponding to the scalar operator (31), which also satisfy the boundary conditions, $\partial_r\phi_n^{\mathrm{sca}}(0) = \phi_n^{\mathrm{sca}}(R) = 0$, are given by,

$$\phi_n^{\mathrm{sca}}(r) \;\equiv\; \sin\left(n\pi r/R\right)/\,r. \tag{37}$$

The corresponding eigenvalues for the operator (31) are given by, $-(n\pi/R)^2$, such that the design matrices read,

$$\mathsf{L}_{dn}^{\mathrm{sca}} \;=\; -\frac{n^2\pi^2}{R^2}\;\mathsf{F}_{dn}^{\mathrm{sca}}, \tag{38}$$

where $\mathsf{F}_{dn}^{\mathrm{sca}} \equiv \phi_n^{\mathrm{sca}}(r_d)$. We should note that by using a collocation method instead of a weak formulation, we do not leverage the orthogonality (in $L^2[0, R]$) of these basis functions. We will explore this in future work.

4 Application: TOV neutron star

We present an application of the method developed in Sections 2 and 3 to a static, spherically-symmetric neutron star described by the Tolman-Oppenheimer-Volkoff (TOV) equations (Tolman, 1939; Oppenheimer

[1] We exclude the trivial root at zero, since this would yield the zero function, which is of no use in a spectral expansion.

and Volkoff, 1939). This is a relatively simple, yet non-trivial, solution of the Einstein equations, so it provides a well-controlled setting to validate the method. The data and code for this application can be found online[2].

The matter distribution in a TOV star is such that E and P are non-zero, while, $\boldsymbol{P} = \mathbf{0}$. As a result, solving equation (2), one can see that $\boldsymbol{X} = \mathbf{0}$. Furthermore, solving equation (5), one can show that $\boldsymbol{\beta} = \mathbf{0}$. Hence, both vector fields vanish and only the scalar equations (3–4) remain to be solved. Since $\boldsymbol{X}$ vanishes, also A vanishes, and the scalar equations reduce to,

$$\boldsymbol{\nabla}^2\psi \;=\; -2\pi\, E/\psi \tag{39}$$

$$\boldsymbol{\nabla}^2\,(\alpha\psi) \;=\; +2\pi\,(\alpha\psi)\,(E+2P)\,/\psi^2 \tag{40}$$

where we assume E and P to be known from the matter distribution of the TOV solution.

We start with equation (39). Since it is non-linear in ψ, we solve it in an iterative way. Substituting the scalar Laplacian (Eq. 31), and introducing $\tilde{\psi}$ (Eq. 35), we find,

$$\left(\partial_r^2 \,+\, \frac{2}{r}\,\partial_r\right)\tilde{\psi}_{(k)} \;=\; -2\pi\, E/\big(\tilde{\psi}_{(k-1)} \,+\, \psi(R)\big), \tag{41}$$

or, equivalently, in discretised form using (Eq. 38),

$$\mathsf{L}^{\text{sca}}\,\boldsymbol{w}^{\psi}_{(k)} \;=\; -2\pi\, E/\big(\mathsf{F}^{\text{sca}}\,\boldsymbol{w}^{\psi}_{(k-1)} \,+\, \psi(R)\big). \tag{42}$$

This can now be solved in an iterative way for $\boldsymbol{w}^{\psi}$. Note that the evaluation of E and the division is implied to be point-wise for each data point. As initial guess, we take $\tilde{\psi}_{(0)} = 0$, and hence $\boldsymbol{w}^{\psi}_{(0)} = \mathbf{0}$. To facilitate the propagation of Gaussian probability distributions, we make a linear approximation of the right-hand side,

$$S_\psi\big[\mathcal{G}\big] \;\approx\; S_\psi\big[\mathcal{G}_0\big] \;+\; \sum_{g\,\in\,\mathcal{G}} \partial_g S_\psi\big[\mathcal{G}_0\big]\,(g-g_0) \tag{43}$$

in which, $\mathcal{G} \equiv \{E, \psi\}$, and the partial derivatives read,

$$\partial_E S_\psi \;=\; -2\pi/\psi, \tag{44}$$

$$\partial_\psi S_\psi \;=\; +2\pi\, E/\psi^2. \tag{45}$$

From this linear approximation, we can approximate the covariance matrix of the right-hand side,

$$\Sigma_{S_\psi} \;=\; \mathsf{J}_E\,\Sigma_E\,\mathsf{J}_E{}^{\mathrm{T}} \;+\; \mathsf{J}_\psi\,\Sigma_\psi\,\mathsf{J}_\psi{}^{\mathrm{T}} \tag{46}$$

where the Jacobians for each variable, g, are defined as,

$$(\mathsf{J}_g)_{db} \;\equiv\; \partial_g S_\psi\big[E, \psi_{(k-1)}\big]\,(r_d)\;\delta_{db}. \tag{47}$$

Note that these are diagonal matrices and that partial derivatives are evaluated using the ψ from the previous iteration. As a result, this covariance matrix will change in every iteration. As a prior, we take a zero-mean Gaussian with a diagonal covariance matrix of the form,

$$\big(\Sigma_{\boldsymbol{w}}\big)_{db} \;=\; \left(\frac{\sigma_{\boldsymbol{w}}}{d^2}\right)^2\;\delta_{db}. \tag{48}$$

All this can now be plugged into Eqs. (21–26) to obtain the posterior distribution over ψ.

[2] github.com/Poincare-code/paper_ProbNum25

Next, we solve equation (40). Substituting the scalar Laplacian (Eq. 31), and introducing $\widetilde{\alpha\psi}$ (Eq. 36), yields,

$$\left(\partial_r^2 \,+\, \frac{2}{r}\,\partial_r\right)(\alpha\psi)_{(k)} \;=\; 2\pi\,(\alpha\psi)_{(k-1)} \times \big(E+2P\big)/\psi^2. \tag{49}$$

or, equivalently, in discretised form using (Eq. 38),

$$\mathsf{L}^{\text{sca}}\,\boldsymbol{w}^{\alpha\psi}_{(k)} \;=\; 2\pi\,\big(\mathsf{F}^{\text{sca}}\,\boldsymbol{w}^{\alpha\psi}_{(k-1)} + (\alpha\psi)(R)\big) \times \big(E+2P\big)/\psi^2 \tag{50}$$

Again, this can be solved in an iterative way for $\boldsymbol{w}_{\alpha\psi}$, multiplication with $\big(E+2P\big)/\psi^2$ is point-wise, and as initial guess, we take $\widetilde{\alpha\psi}_{(0)} = 0$, such that $\boldsymbol{w}^{\alpha\psi}_{(0)} = \mathbf{0}$. The linear approximation of the right-hand side reads,

$$S_{\alpha\psi}\big[\mathcal{G}\big] \;\approx\; S_{\alpha\psi}\big[\mathcal{G}_0\big] \;+\; \sum_{g\,\in\,\mathcal{G}} \partial_g S_{\alpha\psi}\big[\mathcal{G}_0\big]\,(g-g_0) \tag{51}$$

in which, $\mathcal{G} \equiv \{E, P, \psi, \alpha\psi\}$, and the partial derivatives are given by,

$$\partial_E S_{\alpha\psi} \;=\; +2\pi\,(\alpha\psi)/\psi^2, \tag{52}$$

$$\partial_P S_{\alpha\psi} \;=\; +4\pi\,(\alpha\psi)/\psi^2, \tag{53}$$

$$\partial_\psi S_{\alpha\psi} \;=\; -4\pi\,(\alpha\psi)\,\big(E+2P\big)/\psi^3, \tag{54}$$

$$\partial_{\alpha\psi} S_{\alpha\psi} \;=\; +2\pi\,\big(E+2P\big)/\psi^2. \tag{55}$$

Using this linear approximation, we can approximate the covariance matrix of the right-hand side,

$$\Sigma_{S_{\alpha\psi}} \;=\; \mathsf{J}_E\,\Sigma_E\,\mathsf{J}_E{}^{\mathrm{T}} \;+\; \mathsf{J}_P\,\Sigma_P\,\mathsf{J}_P{}^{\mathrm{T}} \;+\; \mathsf{J}_\psi\,\Sigma_\psi\,\mathsf{J}_\psi{}^{\mathrm{T}} \;+\; \mathsf{J}_{\alpha\psi}\,\Sigma_{\alpha\psi}\,\mathsf{J}_{\alpha\psi}{}^{\mathrm{T}}, \tag{56}$$

where the Jacobians for each variable, g, are defined as,

$$(\mathsf{J}_g)_{db} \;\equiv\; \partial_g S_{\alpha\psi}\big[E, P, \psi, (\alpha\psi)_{(k-1)}\big]\,(r_d)\;\delta_{db}. \tag{57}$$

Note that the partial derivatives are evaluated using $\alpha\psi$ from the previous iteration and thus is updated throughout the iterations. As a prior, we use the same covariance (48) as for ψ. Using Eqs. (21–26) we can then obtain the posterior distribution over $\alpha\psi$.

Figure 1 shows the TOV input for the matter and the resulting metric functions. For the standard deviation of the prior for both ψ and $\alpha\psi$, we take $\sigma_{\boldsymbol{w}} = 0.05$. The probability distributions on the matter sources are approximated by Gaussians with means at the TOV values and diagonal covariance functions with standard deviations that are 10% of the function values. We can see the posterior contracting around the true solution. The remaining deviation between the true solution and the posterior mean is due to the large uncertainties on the matter sources and the prior that were chosen.

Figure 2 shows the convergence of the errors and uncertainties in the iterative scheme. The maximum absolute difference (ε) between the PN prediction and the (true) classical solution, and the standard deviation (σ) of the posterior distribution are defined as,

$$\varepsilon_f(k) \;\equiv\; \max_d \big|f_{(k)}(r_d) - f_{\text{TOV}}(r_d)\big|, \tag{58}$$

$$\sigma_f(k) \;\equiv\; \max_d \sqrt{\big(\Sigma_f\big)_{dd}}, \tag{59}$$

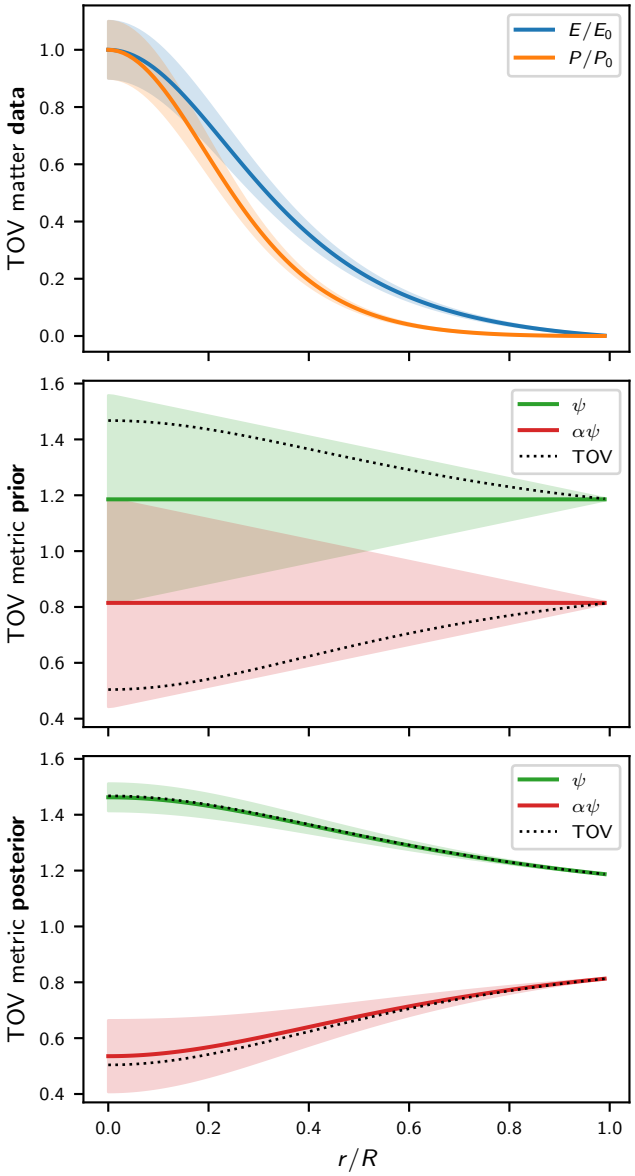

Figure 1: Data, prior, and posterior distributions for the Bayesian solution of the Einstein equations for a TOV star. Shaded regions indicate 1σ confidence intervals. Dotted black lines denote the (true) solution obtained in a classical way.

where we consider the maximum over the data points, $d \in \{1, \dots, D\}$, and, where f_{TOV} is the (true) solution of the relevant variable obtained with a classical solver. Both show similar behavior, decreasing and saturating, suggesting that the posterior variance can be used to estimate the error. However, we should emphasize that we have not yet calibrated the uncertainties in any way.

5 Discussion

The method described above provides a simple approach to solve the Einstein equations in a PN way. However, due to its simplicity, it leaves room for improvement, especially in terms of computational efficiency.

For example, the orthogonality of the basis functions could be leveraged by moving to a weak formulation instead of a collocation method for the spatial discretisation, and their relation to the Fourier basis suggest the use of their Green's functions or methods based on

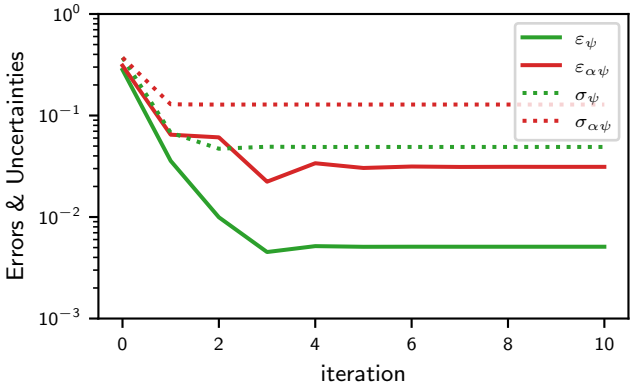

Figure 2: Convergence of the fixed-point iteration schemes. Solid lines denote the maximum absolute difference between the estimate and the (true) classical solution. Dotted lines denote the standard deviation of the posterior distribution.

Fast Fourier Transforms (FFTs) for solving the linear systems involved. Furthermore, several advanced solution methods exist to efficiently solve the Bayesian regression problem (Eqs. 21–26; e.g. Wenger et al., 2022). We will explore these optimisations in future work.

Once we can efficiently obtain the probabilistic solution, the next step would be to leverage the uncertainties to optimise simulations. This could be done, for instance, by minimising the required evaluations of the source functions which are notoriously expensive in NR. In addition, since we expect the metric to be smoother than the matter sources, we can use PN to quantify this and determine, when, where, and at what resolution we need to update the metric in general-relativistic hydrodynamics simulations. These applications of PN to NR will also be explored in future work.

So far, we have not yet leveraged the rich mathematical structure of GR, mainly because we omitted differential geometry and immediately started with a specific formulation of the Einstein equations (2–5). However, we believe that NR has great potential to apply advanced PN methods, because of its rich mathematical structure and symmetries that can be leveraged. Moreover, the probability distributions over the geometry provided by PN could lead to novel ways to study NR.

6 Conclusion

We have explored the potential of probabilistic numerics in numerical relativity. The main goal was to demonstrate the viability of PN in this challenging context. We did this by posing the solution of the Einstein equations as a Bayesian regression problem, specifically, for a waveless approximation to the Einstein equations which only considers the elliptic sector, but which is already of great astrophysical relevance. As a first application, we modelled a posterior distribution over the geometry inside a static and spherically-symmetric neutron star, given uncertain data about the matter distribution inside the star. Given this successful proof-of-principle, we conclude that probabilistic numerics can provide interesting insights in numerical relativity and warrants further exploration.

Acknowledgements

We would like to thank Marvin Pförtner, Nathaël Da Costa, Tim Weiland, and Philipp Hennig for insightful discussions on this topic. This research was supported by the Research Foundation – Flanders (FWO; Grant No. I000725N and I002123N).

References

B. P. Abbott et al. Observation of Gravitational Waves from a Binary Black Hole Merger. *Phys. Rev. Lett.*, 116(6):061102, 2016a. doi: 10.1103/PhysRevLett.116.061102.

B. P. Abbott et al. Tests of General Relativity with GW150914. *Physical Review Letters*, 116:221101, May 2016b. doi: 10.1103/PhysRevLett.116.221101.

B. P. Abbott et al. Tests of general relativity with the binary black hole signals from the LIGO-Virgo catalog GWTC-1. *Physical Review D*, 100(10):104036, Nov. 2019. doi: 10.1103/PhysRevD.100.104036.

L. Blanchet. Post-Newtonian theory for gravitational waves. *Living Reviews in Relativity*, 27(1):4, July 2024. doi: 10.1007/s41114-024-00050-z.

P. C.-K. Cheong, L.-M. Lin, and T. G. F. Li. Gmunu: toward multigrid based Einstein field equations solver for general-relativistic hydrodynamics simulations. *Classical and Quantum Gravity*, 37(14):145015, July 2020. doi: 10.1088/1361-6382/ab8e9c.

P. C.-K. Cheong, A. T.-L. Lam, H. H.-Y. Ng, and T. G. F. Li. Gmunu: paralleled, grid-adaptive, general-relativistic magnetohydrodynamics in curvilinear geometries in dynamical space–times. *Monthly Notices of the Royal Astronomical Society*, 508(2): 2279–2301, Dec. 2021. doi: 10.1093/mnras/stab2606.

J. Cockayne, C. J. Oates, T. J. Sullivan, and M. Girolami. Bayesian Probabilistic Numerical Methods. *SIAM Review*, 61(3):756–789, Jan. 2019. ISSN 0036-1445, 1095-7200. doi: 10.1137/17M1139357.

I. Cordero-Carrión, P. Cerdá-Durán, H. Dimmelmeier, J. L. Jaramillo, J. Novak, and E. Gourgoulhon. Improved constrained scheme for the Einstein equations: An approach to the uniqueness issue. *Physical Review D*, 79:024017, Jan. 2009. doi: 10.1103/PhysRevD.79.024017.

F. De Ceuster, T. Ceulemans, J. Cockayne, L. Decin, and J. Yates. Radiative transfer as a Bayesian linear regression problem. *Monthly Notices of the Royal Astronomical Society*, 518(4):5536–5551, Feb. 2023. doi: 10.1093/mnras/stac3461.

A. Einstein. Die Grundlage der allgemeinen Relativitätstheorie. *Annalen der Physik*, 354:769–822, Jan. 1916. doi: 10.1002/andp.19163540702.

P. Hennig, M. A. Osborne, and M. Girolami. Probabilistic numerics and uncertainty in computations. *Proceedings of the Royal Society A: Mathematical, Physical and Engineering Sciences*, 471(2179):20150142, July 2015. doi: 10.1098/rspa.2015.0142.

P. Hennig, M. A. Osborne, and H. P. Kersting. *Probabilistic Numerics: Computation as Machine Learning*. Cambridge University Press, Cambridge, 2022. doi: 10.1017/9781316681411.

J. A. Isenberg. Waveless Approximation Theories of Gravity. *International Journal of Modern Physics D*, 17:265–273, Jan. 2008. doi: 10.1142/S0218271808011997.

M. Ishak. Testing general relativity in cosmology. *Living Reviews in Relativity*, 22(1):1, Dec. 2018. doi: 10.1007/s41114-018-0017-4.

M. Maggiore, C. V. D. Broeck, N. Bartolo, E. Belgacem, D. Bertacca, M. A. Bizouard, M. Branchesi, S. Clesse, S. Foffa, J. García-Bellido, S. Grimm, J. Harms, T. Hinderer, S. Matarrese, C. Palomba, M. Peloso, A. Ricciardone, and M. Sakellariadou. Science case for the Einstein telescope. *Journal of Cosmology and Astroparticle Physics*, 2020(03):050, Mar. 2020. doi: 10.1088/1475-7516/2020/03/050.

W. I. Newman and N. D. Hamlin. Primitive Variable Determination in Conservative Relativistic Magnetohydrodynamic Simulations. *SIAM Journal on Scientific Computing*, 36(4):B661–B683, Jan. 2014. doi: 10.1137/140956749.

J. R. Oppenheimer and G. M. Volkoff. On Massive Neutron Cores. *Physical Review*, 55:374–381, Feb. 1939. doi: 10.1103/PhysRev.55.374.

M. Pürrer and C.-J. Haster. Gravitational waveform accuracy requirements for future ground-based detectors. *Physical Review Research*, 2(2):023151, May 2020. doi: 10.1103/PhysRevResearch.2.023151.

R. C. Tolman. Static solutions of Einstein's field equations for spheres of fluid. *Phys. Rev.*, 55:364–373, 1939. doi: 10.1103/PhysRev.55.364.

J. Wenger, G. Pleiss, M. Pförtner, P. Hennig, and J. P. Cunningham. Posterior and computational uncertainty in Gaussian processes. In *Advances in Neural Information Processing Systems (NeurIPS)*, 2022.

C. M. Will. The Confrontation between General Relativity and Experiment. *Living Reviews in Relativity*, 17(1):4, June 2014. doi: 10.12942/lrr-2014-4.

J. R. Wilson and G. J. Mathews. In *Frontiers in numerical relativity*, page 306. Cambridge University Press, 1989.